Journal of
Marine Science and Engineering

MDPI

Article

Experimental Study on the Probability of Different Wave Impact Types on a Vertical Wall with Horizontal Slab by Separation of Quasi-static Wave Impacts

Jianjun Huang [1,2,*], Guoping Chen [2] and Ryan J. Lowe [3]

[1] Oceans Graduate School, The University of Western Australia, Perth 6009, Australia
[2] College of Harbour Coastal and Offshore Engineering, Hohai University, Nanjing 210098, China; gpchen1965@163.com
[3] UWA Oceans Institute, The University of Western Australia, Perth 6009, Australia; ryan.lowe@uwa.edu.au
* Correspondence: jianjun.huang@research.uwa.edu.au or huang_jianjun_1995@126.com

Abstract: When the fundamental natural frequency of marine structures is comparable to the dominant frequency of incident waves, the response of the load on the structure will be amplified. Accurately quantifying how wave loads can be amplified by incident wave conditions must thus be considered in any structural analysis, given how sensitive these characteristics are to different wave impact types. Systematic physical model tests of wave impacts on the simple horizontal plate and the vertical wall with a horizontal overhanging cantilever slab were performed. By first comparing quasi-static wave load estimates along a simple horizontal plate (obtained by low-pass filtering the pressure time series at different cut-off frequencies) with quasi-static uplift pressures from established predictive formulations, a cut-off frequency of 7 Hz was found to accurately separate the quasi-static component from impulsive wave impacts. By applying the low-pass filtering approach with the selected cut-off frequency to the pressure measurements for the vertical wall with a horizontal cantilever slab case, the impulsive and quasi-static peaks were attained, which were then used to quantify the probabilities of individual impulsive, dynamic, and quasi-static wave impacts. Incoming wave conditions and structural clearance had a significant effect on the probabilities of different wave impacts. With the increasing wave height and wave steepness, wave impacts on the horizontal slab and vertical wall were increasingly of the impulsive type and less frequently of the quasi-static type, while the probability of dynamic impact types were relatively stable. As the overhanging slab was shifted from elevated to submerged, the dominant type of wave impact on the structure was variable, ranging from impulsive to dynamic to quasi-static as its elevation was lowered. The results indicated that up to 90% of the impacts were of the impulsive type when the overhanging slab was on or slightly over the still water level. Moreover, the presence of the vertical wall increased the magnitude of wave loads and the occurring frequency of impulsive wave impacts for the horizontal slab.

Keywords: wave impact type; cut-off frequency; occurring probability; structural clearance

Citation: Huang, J.; Chen, G.; Lowe, R.J. Experimental Study on the Probability of Different Wave Impact Types on a Vertical Wall with Horizontal Slab by Separation of Quasi-static Wave Impacts. *J. Mar. Sci. Eng.* **2022**, *10*, 615. https://doi.org/10.3390/jmse10050615

Academic Editor: Constantine Michailides

Received: 16 March 2022
Accepted: 27 April 2022
Published: 30 April 2022

1. Introduction

There has been a growing need to build a range of different structures in the ocean to support the blue economy and coastal population growth, with these structures expected to be increasingly vulnerable to the impacts of climate change, including sea level rise and the changing frequency and intensity of extreme storms [1–7]. As a result, studies on the dynamic interactions between wave-driven ocean processes and coastal/offshore structures are vital, given how wave impacts affect coastal protection and the safety of marine structures.

How to reasonably predict and determine the wave loads is required for designing coastal and offshore structures, with specific loading dependent on both the incoming wave conditions and the geometry of the structure. For the vertical structures, incoming

wave shapes and breaking conditions play a dominant role in determining the wave impact [8–10], with the maximum wave load mostly associated with the thin air layer between the wave front and the structural surface, called flip-through, specifically [11–13]. It has also been found that the largest local wave impacts usually occur at positions near the still water level [14–17]. To date, the most widely recognized empirical formula to predict wave loads on vertical wall is from study by Goda [18], which has been widely applied to ocean engineering applications. Wave loads due to vertical wave motion on horizontal structures (such as coastal bridges and pile-supported platforms) have been increasingly studied [19,20]. In addition to the wave condition, the uplift wave load shows the significant response to the elevation difference between the bottom of a horizontal structure and the still water level (termed structural clearance) [21–23]. During an extreme wave attack (such as tsunami and typhoon-induced freak waves), structural failure has commonly been found to occur on the horizontal parts of the structure [3,5,24,25]. Recently, an increasing number of marine structures with complicated forms have been developed (such as surge barriers, flood gates, sluice gates, dewatering sluices, lock gates, and crest walls), and have been modeled as a combination of a vertical wall with overhangs [25–31]. For such hybrid structures, the roles of wave conditions and structural geometry on wave loads have been studied to a lesser extent. Recently, De Almeida and Hofland investigated how the roles that variable wave fields and entrapped air play in controlling the standing wave impacts on vertical hydraulic structures with overhangs [32–34]. Based on physical model tests, Huang and Chen [35,36] proposed that the maximum wave impact on the horizontal cantilever slab occurred when the structural clearance is approximately 0.2 times the incoming significant wave height, and further presented the relationships between the wave impact rising time, the wave impact frequency, and the wave load.

However, when designing marine structures subject to waves, the maximum wave load is not the only relevant factor; dynamic effects must also be considered in the structural analysis, otherwise the analysis will overestimate or underestimate the actual reaction load on the structure. When the dominant frequency of incident waves is much smaller than the fundamental natural frequency of marine structures, a static analysis is usually sufficient to attain the designed structural response to incident waves [37]. Nevertheless, if the natural frequency of the structure is close to the wave frequency, particularly in cases in which the marine structures are more flexible, the actual response load on the structure can be significantly amplified due to resonance, such that a dynamic analysis must be conducted [38,39]. Generally, using the product of incident wave loads and the dynamic magnification factor to reflect the actual dynamic response of marine structures impacted by extreme waves is a widely accepted approach [31]. Huang and Chen investigated the structural response analysis with wave loads through the finite element method, and found that the dynamic magnification factor could be either larger than 1.0 or smaller than 1.0, representing the respective underestimation or overestimation of wave loads when ignoring the dynamic characteristic of wave loads [36]. While the wave force measurements have included the structure response and are not suitable for dynamic amplification effect analysis, the wave pressures contain the significantly impulsive property and are as important and necessary as the wave forces for marine structure design, particularly for specific parts, because different parts of the entire structure will be faced with different magnitudes of the wave loads, such as the wave pressures on the deck, beam, or pile. Given that the dynamic characteristic of a wave load (i.e., the dynamic magnification factor) is sensitive to different wave impact types, it is thus key to distinguish different wave impact types and investigate how frequently they occur on structures, the latter of which has been investigated to a lesser extent. In addition, the roles that wave conditions and structure parameters have in determining the probability of different wave impact types has been rarely considered in the literature. Given this, a series of model tests of two configurations (a simple horizontal plate and a vertical wall with a horizontal overhanging cantilever slab) were performed in a wave flume, and the wave pressures on different locations were measured. Firstly, based on the model tests of the simple horizontal plate, a suitable cut-off frequency to

separate the quasi-static wave load from impulsive wave load was identified. Then, by applying the low-pass filtering method with the selected cut-off frequency to classify the wave impact types for the vertical wall with a horizontal cantilever slab, the influence of different wave conditions and structural clearances on the probability of three types of wave impact (impulsive, dynamic, or quasi-static) were investigated.

This paper is structured as follows. In Section 2, a detailed overview of the experimental setup is provided, including the physical model setup, instrumentation, and methods of data processing. The experimental results and discussion are then provided in Section 3. This includes assessing the influences of wave conditions and structural clearance on the probability of different types of wave impact loads. Finally, the conclusions and implications for engineering design are presented in Section 4.

2. Methods

2.1. Experimental Setup

The physical modeling experiment was conducted within a glass-walled wave flume at the Channel Laboratory of Hohai University, P. R. China. The wave flume was 80 m long, 1 m wide, and 1.5 m deep, with waves generated using a piston-type wavemaker with an active wave absorption system to reduce reflected waves at the generation source (Figure 1). In total, two model configurations were evaluated in this study: configuration C1, consisting of a simple horizontal plate; and configuration C2, consisting of a vertical wall with an overhanging horizontal cantilever slab (C2), as shown in Figure 2a,b, respectively. Both model configurations were built approximately 50 m away from the wavemaker at a 1:30 geometric scale, with a Froude number similarity adopted to reproduce the wave-driven hydrodynamic processes. At the model scale, the vertical wall was 0.65 m high and the horizontal plate (slab) was 0.50 m long (equivalent to 19.5 m and 15 m at the prototype scale, respectively). The physical models were constructed from rigid acrylic sheets, with the horizontal plate (slab) connected to a steel frame that enabled the plate (slab) to be adjusted vertically to vary the structural clearance c (i.e., the elevation difference between the bottom of horizontal plate and the still water level). During the experiments, the clearance c was varied between −0.10 m and 0.10 m (equivalent to −3.0 to +3.0 m at the prototype scale), where positive values represented cases when the horizontal plate was above the still water level. Further details on the physical model and wave flume are provided in the study by Huang and Chen [35], and are only summarized here.

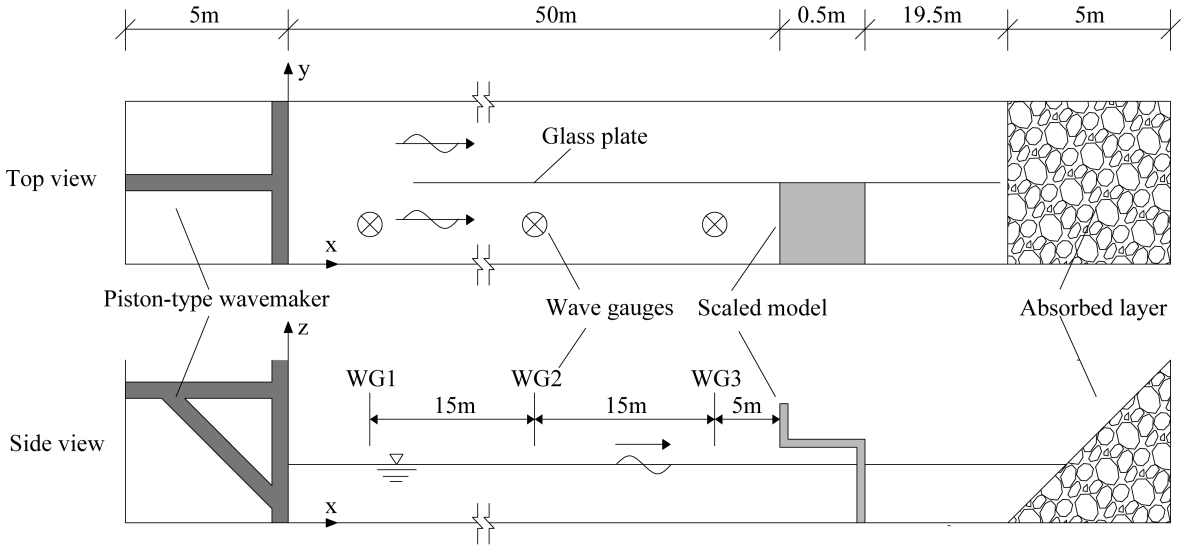

Figure 1. Experimental setup in the wave flume.

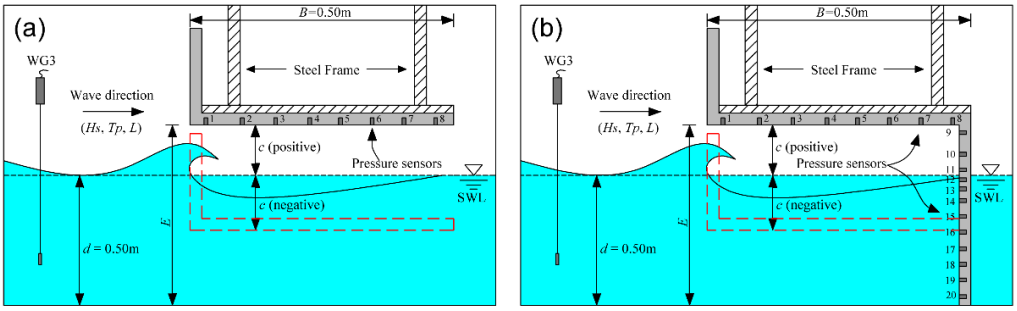

Figure 2. Two configurations of tested physical models; (**a**) the simple horizontal slab; (**b**) the vertical wall with overhanging horizontal cantilever slab.

2.2. Wave Conditions and Experimental Measurements

Based on the prototype (field) wave conditions on which the model testing was based, a series of irregular wave conditions was generated for a range of significant wave heights H_s between 0.05 and 0.15 m using a constant peak period of T_p = 1.45 s, based on a JONSWAP spectrum with a peak enhancement factor of γ = 3.3. For a summary of all the wave conditions and structural clearances used in the experiments, refer to Table 1. At the prototype (field) scale, this was equivalent to H_s between 1.5 and 4.5 m at a fixed period of T_p = 7.94 s. The water depth in the flume was held constant at 0.50 m during all experiments (equivalent to a 15 m depth at the prototype scale), with the structural clearance c varied by raising/lowering the models in the flume. Based on the wave peak period T_p = 1.45 m used in the testing, the wavelength in the flume (inferred from linear wave theory) was L = 3.28 m. A total of 35 wave trials were conducted (denoted T1 to T35), with five of the conditions (denoted T16 to T20) repeated to include both the simple horizontal slab configuration (C1) and the vertical wall with an overhang configuration (C2) (Table 1).

Table 1. Summary of conditions used in the wave trials.

Trial	c (m)	H_s (m)	T_p (s)	Tested Configurations	Trial	c (m)	H_s (m)	T_p (s)	Tested Configurations
T1	−0.1	0.05	1.45	C2	T19	0	0.125	1.45	C1, C2
T2	−0.1	0.075	1.45	C2	T20	0	0.15	1.45	C1, C2
T3	−0.1	0.1	1.45	C2	T21	0.02	0.05	1.45	C2
T4	−0.1	0.125	1.45	C2	T22	0.02	0.075	1.45	C2
T5	−0.1	0.15	1.45	C2	T23	0.02	0.1	1.45	C2
T6	−0.05	0.05	1.45	C2	T24	0.02	0.125	1.45	C2
T7	−0.05	0.075	1.45	C2	T25	0.02	0.15	1.45	C2
T8	−0.05	0.1	1.45	C2	T26	0.05	0.05	1.45	C2
T9	−0.05	0.125	1.45	C2	T27	0.05	0.075	1.45	C2
T10	−0.05	0.15	1.45	C2	T28	0.05	0.1	1.45	C2
T11	−0.02	0.05	1.45	C2	T29	0.05	0.125	1.45	C2
T12	−0.02	0.075	1.45	C2	T30	0.05	0.15	1.45	C2
T13	−0.02	0.1	1.45	C2	T31	0.1	0.05	1.45	C2
T14	−0.02	0.125	1.45	C2	T32	0.1	0.075	1.45	C2
T15	−0.02	0.15	1.45	C2	T33	0.1	0.1	1.45	C2
T16	0	0.05	1.45	C1, C2	T34	0.1	0.125	1.45	C2
T17	0	0.075	1.45	C1, C2	T35	0.1	0.15	1.45	C2
T18	0	0.1	1.45	C1, C2					

During the experiments, water elevations were recorded along the flume at three locations (WG1–WG3) using capacitance wave gauges with a sampling rate of 100 Hz (DJ800, from the China Institute of Water Resources and Hydropower Research), with the incoming significant wave height defined based on the measurements at the first wave gauge (WG1) (Figure 2, Table 2). The distances between these three wave gauges were

determined for the separation of the incident and reflection waves [40,41]. To measure the wave impact pressures, 20 pressure sensors (WMS-51P2J0L2M0, from Xi'an Microsensitive Instrument and Meter Co. Ltd., Xi'an, China) located in the center axis of the tested part of the flume were embedded in the surfaces of the horizontal plate and vertical wall through the reserved ports (see Figure 2). A total of 8 pressure sensors were installed on horizontal plate or slab (PS1 to PS8), while the other pressure sensors were located on the vertical wall (PS12 to PS20), with data recorded at a sampling rate of 5000 Hz.

Table 2. The locations of different instruments.

Instrument Description	Instrument	x (m)	y (m)	z (m)
Wave paddle	WP	0	-	-
Wave gauge	WG1	15	0.25	-
Wave gauge	WG2	30	0.25	-
Wave gauge	WG3	45	0.25	-
Pressure sensor (overhanging horizontal cantilever slab)	PS1	50.015	0.25	0.4–0.6
Pressure sensor (overhanging horizontal cantilever slab)	PS2	50.095	0.25	0.4–0.6
Pressure sensor (overhanging horizontal cantilever slab)	PS3	50.155	0.25	0.4–0.6
Pressure sensor (overhanging horizontal cantilever slab)	PS4	50.215	0.25	0.4–0.6
Pressure sensor (overhanging horizontal cantilever slab)	PS5	50.275	0.25	0.4–0.6
Pressure sensor (overhanging horizontal cantilever slab)	PS6	50.355	0.25	0.4–0.6
Pressure sensor (overhanging horizontal cantilever slab)	PS7	50.415	0.25	0.4–0.6
Pressure sensor (overhanging horizontal cantilever slab)	PS8	50.475	0.25	0.4–0.6
Pressure sensor (vertical wall)	PS9	50.48	0.25	0.59
Pressure sensor (vertical wall)	PS10	50.48	0.25	0.54
Pressure sensor (vertical wall)	PS11	50.48	0.25	0.51
Pressure sensor (vertical wall)	PS12	50.48	0.25	0.49
Pressure sensor (vertical wall)	PS13	50.48	0.25	0.47
Pressure sensor (vertical wall)	PS14	50.48	0.25	0.44
Pressure sensor (vertical wall)	PS15	50.48	0.25	0.39
Pressure sensor (vertical wall)	PS16	50.48	0.25	0.33
Pressure sensor (vertical wall)	PS17	50.48	0.25	0.27
Pressure sensor (vertical wall)	PS18	50.48	0.25	0.21
Pressure sensor (vertical wall)	PS19	50.48	0.25	0.12
Pressure sensor (vertical wall)	PS20	50.48	0.25	0.03

2.3. Data Processing

Wave pressures were recorded synchronously; Figure 3 presents an example time series of wave pressures on the horizontal plate (C1) for wave trial T12, showing a typical larger impulsive wave pressure of short duration followed by a smaller quasi-static wave pressure with a long duration. The wave pressures were not distributed uniformly on the bottom of horizontal plate, with some degree of randomness and scatter between various pressure sensors (PS1–PS8). Similar to the significant wave height, $P_{1/3}$ was defined as the significant wave pressure for each time series of wave load (pressure), using a zero up-crossing method. In addition, the average of the highest 1% of the wave pressure $P_{1/100}$ was also quantified. Due to the variability of wave pressures across different pressure sensors, the results are presented using the average wave pressures for both the horizontal slab (PS1–PS8) and vertical wall (PS9–PS20) sensors.

Over an individual wave period, the pressure time series was characterized by an initially large impact wave pressure P_{im}, followed by a more slowly varying quasi-static uplift wave pressure P_{qs+} (Figure 3). Based on previous studies of wave loads on vertical walls [42,43], and as summarized in Table 3, when the ratio of the impact wave pressure P_{im} to the quasi-static uplift wave pressure P_{qs+} (i.e., P_{im}/P_{qs+}) was larger than 2.5, the corresponding wave impact process was defined as an 'impulsive' type; when $P_{im}/P_{qs+} < 1.2$, the wave impact was of a 'quasi-static' type; and for intermediate values ($1.2 < P_{im}/P_{qs+} < 2.5$), the wave impact was classified as a 'dynamic' type.

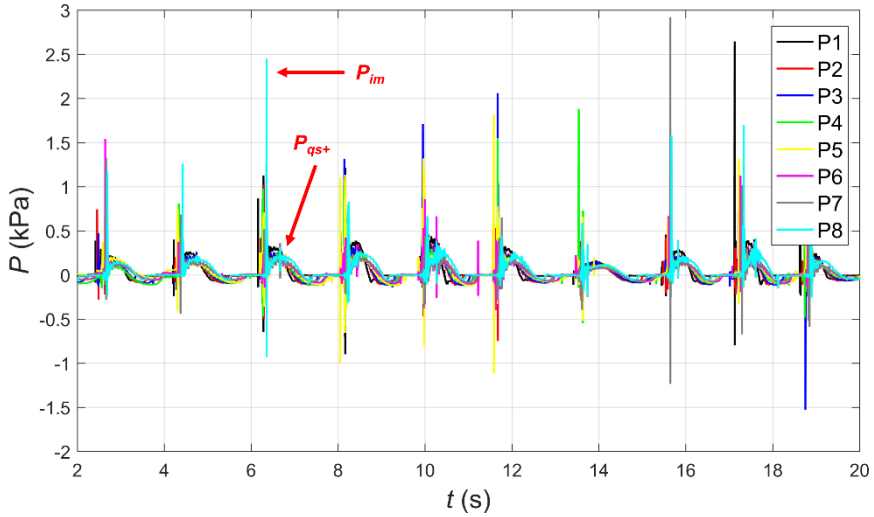

Figure 3. Example time series of wave pressures recorded on horizontal plate for trial T12.

Table 3. Classification of wave impact types.

P_{im}/P_{qs+}	Wave Impact Types
>2.5	Impulsive
1.2–2.5	Dynamic
<1.2	Quasi-static

For a given wave's time series, the total number N of individual wave impacts was grouped into the three wave impact types, $N = A + B + C$, where A is the number of impulsive wave impacts, B is the number of dynamic wave impacts, and C is the number of quasi-static wave impacts in series. Thus, the probability of three such types of wave impact could be calculated as follows: $PRO_{im} = A/N$, $PRO_{dyn} = B/N$, and $PRO_{qs+} = C/N$, where PRO_{im}, PRO_{dyn}, PRO_{qs+} represent the probability of impulsive, dynamic, and quasi-static wave impact, respectively.

3. Results and Discussion

3.1. Role of Cut-Off Frequency for Separation of Quasi-static Wave Impacts from Impulsive Wave Impacts

Several methods have been successfully used to separate the quasi-static component from the impulsive wave impacts [31,44–46], among which the low-pass filtering approach with a cut-off frequency was adopted in this study. By conducting the model test of the simple horizontal plate (C1), the role of the cut-off frequency in the separation of the quasi-static wave impact from the impulsive wave impact was first investigated. In the example wave impact (pressure) time series in Figure 3, it is visually possible to identify the separate contributions of both the impulsive and quasi-static components of the total load time series. To decompose the impact wave pressure P_{im} and quasi-static uplift wave pressure P_{qs+}, an approach to separate these two types of wave loads first needed to be established. Prior studies that examined these wave impacts indicated that the impulsive wave load was always associated with higher frequency fluctuations; whereas the quasi-static wave load occurred at lower frequencies, indicating the importance of different time scales when distinguishing between these impulsive and quasi-static processes. Thus, it is common to apply low-pass filtering methods to isolate the quasi-static load component from the pressure time series [31,35]. However, until now, how to optimally choose the cut-off frequency within the low-pass filtering still remains an open question. In practice, studies to date have subjectively chosen the cut-off frequency based on a specific given data set. In this section, we used results from the subset of model testing of the horizontal plate (C1) to

conduct a detailed assessment of how the choice of the cut-off frequency influenced the separation of the contributions of these two types of wave impact.

Through application of low-pass filtering from continuous 1D wavelet transform (CWT) [47], the time series of the separated quasi-static (low-frequency) component of wave pressure on the bottom of the horizontal plate was compared against known responses from predictive formulations. Given that different cut-off frequency values can rebuild different time series of quasi-static wave load and thus different significant wave pressure $P_{1/3}$, Figure 4 shows an example for pressure sensor PS1 of the horizontal plate within wave trial T12, in which the significant wave pressure $P_{1/3}$ varied with the cut-off frequency f_c. As shown in the figure, when the cut-off frequency f_c increased, $P_{1/3}$ initially increased and then reached an approximately constant value. For cut-off frequencies f_c larger than ~2000 Hz, the significant wave pressure $P_{1/3}$ was not sensitive to higher values of f_c. In order to further investigate the role that cut-off frequency played in separating impulse and quasi-static wave impacts, these low-pass-filtered load measurements could then be compared against the predictive formulations for estimating quasi-static wave impacts on horizontal plates. Cuomo et al. [24] conducted a comprehensive set of physical model tests for horizontal plates exposed to different regular wave conditions and structural clearances, and developed an empirical formula for predicting the quasi-static uplift wave pressure, as follows:

$$\frac{P_{qs+}}{\rho g H_s} = 7.34\eta^{*3} - 5.47\eta^{*2} + 1.18\eta^{*} + 0.42 \quad (1)$$

$$\eta^{*} = \frac{\eta_{max}}{d} \quad (2)$$

where ρ is the density of water, g is the gravitational acceleration, H_s is the corresponding incoming significant wave height (defined as 0.56 times the maximum regular wave height in Cuomo's study [24]), η^* is the normalized hydrostatic head, η_{max} is the maximum wave crest height, c is the structural clearance, and d is the still water depth.

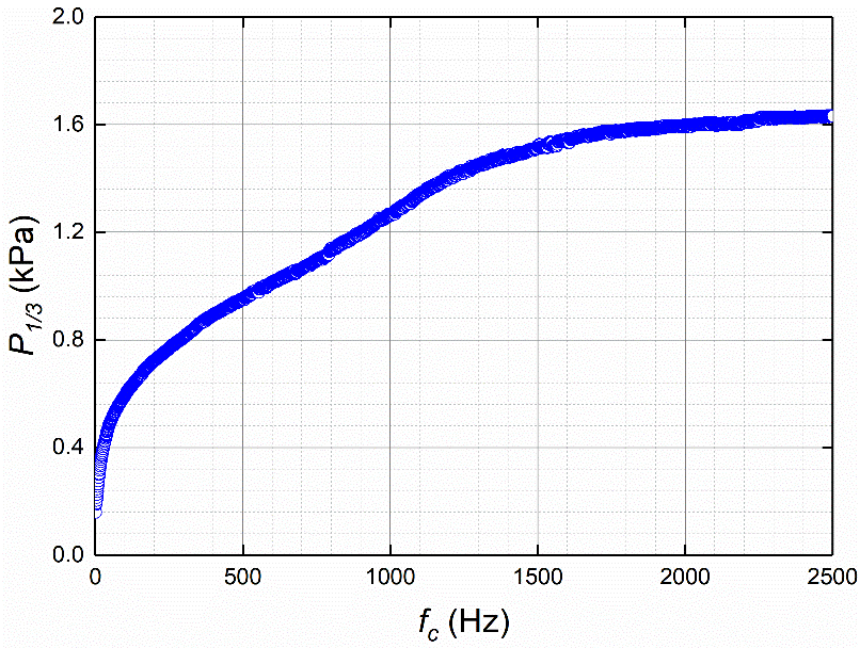

Figure 4. Significant wave pressure $P_{1/3}$ of reconstructed wave load time series on PS1 changed with cut-off frequencies f_c.

Based on Equations (1) and (2), the predicted values of the quasi-static uplift wave pressure $P_{qs+,cal}$ calculated for wave trials T16, T17, T18, T19, and T20 are given in Table 4. Given that η_{max} within Equation (1) corresponded to regular waves, for irregular waves, the maximum crest height for each individual wave is time-varying, and η_{max} is defined here

by the average of the highest 1% of the waves (denoted $\eta_{1/100}$). To build the relationship between the normalized wave crest height and the significant wave height, Figure 5 shows the wave crest height $\eta_{1/100}$ varied with the incoming significant wave height H_s, plotted in both dimensional and nondimensional forms. Note that there were only a few data points within the present wave trials (T16–T20), thus this relationship between $\eta_{1/100}$ and H_s was established by incorporating additional irregular wave model tests, which are plotted together in Figure 5. There was an approximately 1:1 linear positive correlation between H_s and $\eta_{1/100}$, with correlation coefficients larger than 0.90. Due to $\eta_{1/100}$ related to wave amplitude, this suggested that $H_{1/100}$ was about twice H_s, consistent with the Rayleigh distribution of irregular wave height. Based on the nondimensional relation between H_s and $\eta_{1/100}$, Equation (2) can be further used to relate η^* to the wave and structural clearance as follows:

$$\eta^* = \frac{0.88H_s - c}{d} + 0.01 \quad (3)$$

Table 4. Comparison between calculated and measured results.

Wave Trials	Calculated Values from Equation (1)	Measured Values $P_{1/3}$ from Model Tests (kPa)					
	$P_{qs+,cal}$ (kPa)	f_c = 5 Hz	f_c = 6 Hz	f_c = 7 Hz	f_c = 8 Hz	f_c = 9 Hz	f_c = 10 Hz
T16	0.24	0.21	0.23	0.24	0.25	0.26	0.27
T17	0.37	0.34	0.36	0.37	0.39	0.40	0.42
T18	0.49	0.41	0.43	0.46	0.48	0.50	0.52
T19	0.60	0.57	0.59	0.61	0.63	0.66	0.68
T20	0.71	0.65	0.68	0.71	0.74	0.76	0.78

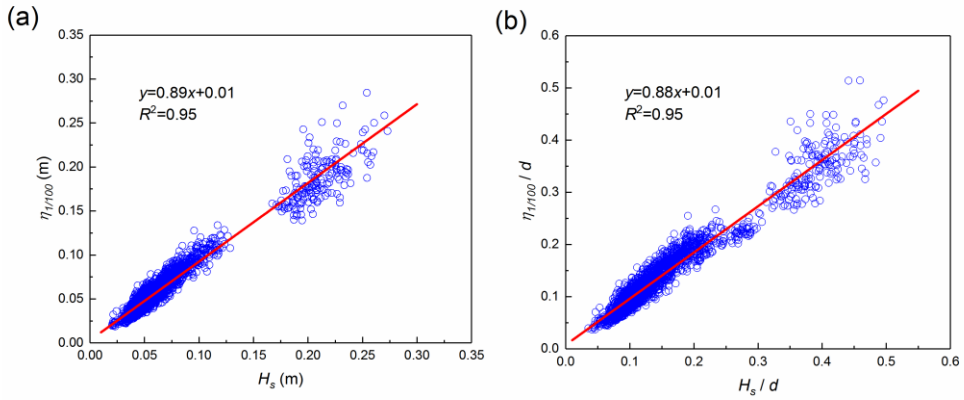

Figure 5. Relationship between the incoming significant wave height H_s and characteristic wave crest height $\eta_{1/100}$ in (**a**) dimensional form and (**b**) nondimensional form.

Given the significant wave height H_s in the denominator of Equation (1), the significant wave pressure $P_{1/3}$ of the rebuilt pressure time series for each wave trial (T16–T20) was compared with the predicted quasi-static uplift wave pressure $P_{qs+,cal}$, as shown in Table 4. Figure 6 shows the ratio of $P_{1/3}/P_{qs+,cal}$ against the cut-off frequency f_c. The ratio $P_{1/3}/P_{qs+,cal}$ increased with the increasing cut-off frequency due to the inclusion of more higher frequency variability in the pressure time series. The meeting crossing point between $P_{1/3}/P_{qs+,cal}$ and 1.0 appeared around f_c = 7 Hz. For this cut-off frequency f_c = 7 Hz, Figure 7 plots the $P_{1/3}$ against $P_{qs+,cal}$ with the corresponding root-mean-square errors (RMSE) and correlation coefficients (R^2) included. Both matched well with each other, with a small RMSE = 0.014 kPa and a high R^2 = 0.99, revealing the good performance of a cut-off frequency equal to 7 Hz for separating the quasi-static component of the load. Compared with a previous work [35], in which the authors subjectively decided to utilize the cut-off frequency of 8 Hz to reconstruct the quasi-static wave load through visual contrasting, the present study provides a more precise and convincing analysis and discussion to support

the final selection. Furthermore, it was also generally consistent with the observation of Xiang et al. [48] that a cut-off frequency of 7.5 Hz could reconstruct the quasi-static component of the wave impact reasonably well. Finally, in Figure 8, the decomposed time series of the impulsive wave impact and quasi-static wave impact are plotted together for f_c = 7 Hz. The quasi-static wave impact appeared to match the expected variability of the quasi-static component of original wave impact well, not only for heavily impulsive processes (the first three individual waves), but also for weakly impulsive ones (the middle four individual waves).

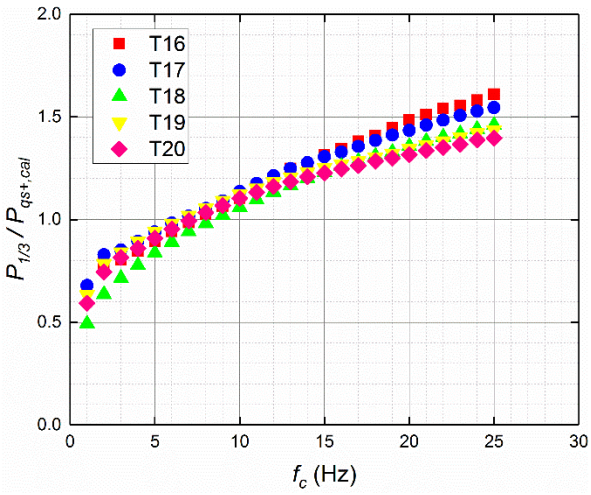

Figure 6. The ratio of the measured averaged values $P_{1/3}$ and calculated values $P_{qs+,cal}$ as a function of different cut-off frequencies f_c for five horizontal wave plate trials.

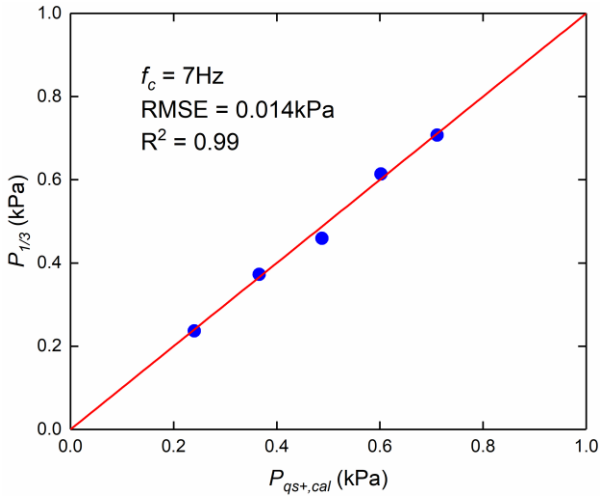

Figure 7. Comparisons between measured values $P_{1/3}$ of rebuilt pressure time series results and calculated values $P_{qs+,cal}$ from empirical formula for a cut-off frequency of 7 Hz.

The separation method using the specific cut-off frequency f_c = 7 Hz was subsequently extended to the vertical wall with overhangs (C2) trials, with an example shown in Figure 9 (for PS1 and PS9 in trial T12, respectively). As shown in Section 3.4, the presence of the vertical wall could significantly enhance the wave impacts on the slab, which was due to the interactions between the wave-induced flow accelerations and the entrapped air within the relative confined space formed from the slab and vertical wall. However, different from the impulsive wave impact processes and the peak impulsive pressure values that were greatly affected by the entrapped air [46], the quasi-static processes seemed to be not significantly sensitive to the entrapped air [33], and thus the selected cut-off frequency representing the upper limitation of low-pass filtering from the horizontal plate tests could be reasonably

adopted in the vertical wall with overhangs, particularly under the similar incident wave conditions. In addition, the cut-off frequency of 7 Hz in this study was used for measured wave pressure low-pass filtering, and was thus of course at the model scale (about 1/10 of the wave period). At the 1:30 geometric scaling used in the experiment, according to the Froude scaling of timescales, this would suggest a cut-off frequency at the prototype scale of ~1 Hz. Nevertheless, from these experiments alone, it was not possible to definitely confirm how these cut-off frequencies would scale between model and field (prototype) scales, as this would have required a focus on quantifying scale effects to specific applications. This is a topic that is as important as the scale effect of the wave loads, but was not the major target in this research; both topics need much more dedicated studies in the future. In the present study, based on the classification approach described in Section 2.3, we aimed to further investigate the probability of different wave impact types (impulsive, dynamic, and quasi-static) on the vertical wall with overhangs, as presented in the following sections.

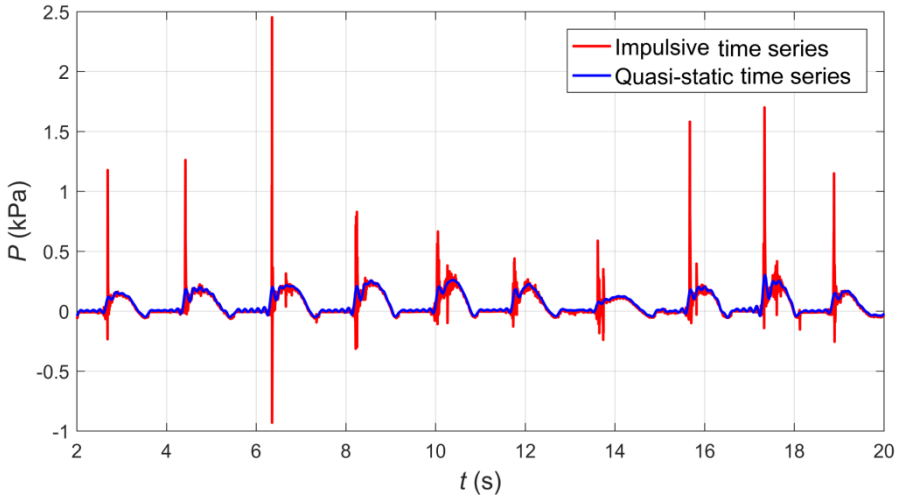

Figure 8. Time series of the decomposed impulsive wave pressure and quasi-static wave pressure of PS1 for the simple horizontal plate (C1).

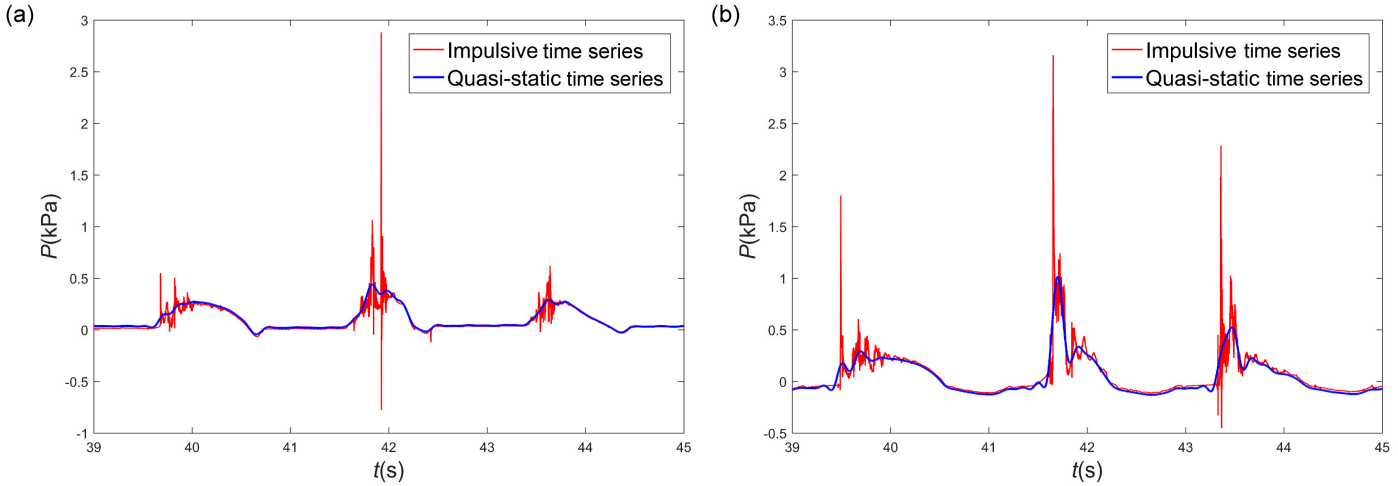

Figure 9. Time series of the decomposed impulsive wave pressure and corresponding reconstructed quasi-static wave pressure for the vertical wall with horizontal cantilever slab (C2) for measurements at (**a**) pressure sensor PS1 and (**b**) pressure sensor PS9.

3.2. Effect of Wave Conditions on the Probabilities of Different Wave Impacts Occurring

Based on the complete series of model tests (total of 35 wave trials, Table 1), the influence of the incoming wave conditions and structural clearance on the probabilities of

various wave impact types (i.e., impulsive, dynamic, and quasi-static) on the vertical wall with an overhanging horizontal cantilever slab were investigated.

For the horizontal cantilever slab portion of the C2 model, the incoming wave height played an important role in the severity of the wave impact. The response of the probability of different wave impacts as a function of incoming wave height H_s is shown in Figure 10 for trials with a structural clearance c = 0.02 m (trials T21–T25). Given that the wave impact on the bottom of the horizontal slab was distributed unevenly among the pressure sensors, values for both the different pressure sensors (scatter points) and averaged ones (solid gray line) are included. Along the horizontal axis, the incoming significant wave height was normalized by the still water depth, expressed as relative wave height H_s/d. Due to the rapid vertical motion of the wave surface, the largest contributions to the wave impacts on the horizontal slab were due to the high frequency (impulse wave impact) contributions. It can thus be seen that the probability of impulsive wave impact PRO_{im} was always higher than 75%, and increased up to about 95% when the wave height was larger. In contrast, the probability of quasi-static loads PRO_{qs+} continuously decreased from 20% to 2% as H_s/d decreased. Such a small proportion of PRO_{qs+} was attributed to another mechanism of wave impact, in which the propagating wave turned into a vertical jet when impacting the vertical wall, and grew into a horizontal jet along the bottom of the horizontal slab. At intermediate time scales, the probability of the dynamic wave impact PRO_{dyn} was relatively independent of H_s/d, ranging from 2% to 4%. For comparison, Figure 11 presents another case for clearance equal to $c = -0.02$ m (trials T11–T15) in which the horizontal slab was below the still water level. Generally, the general trends in the probability for different wave impact types was similar to c = 0.02 m, where PRO_{im} increased, PRO_{qs+} decreased, and PRO_{dyn} was more constant with increases in H_s/d. However, the magnitude of PRO_{im} was reduced, while that of PRO_{dyn} increased, as a result of weaker wave impacts when the slab is submerged. Note that the proportion of PRO_{qs+} remained largely unchanged (always below 20%); thus, the increase in PRO_{dyn} with H_s/d was mostly compensated by the reduction in PRO_{im}.

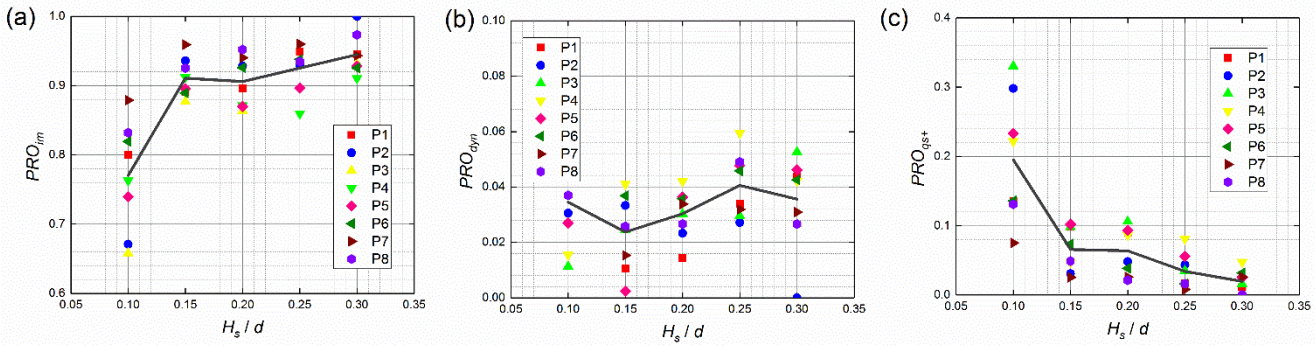

Figure 10. Influence of relative wave height on the probabilities of three types of wave impact on horizontal slab for structural clearance of 0.02 m (trials T21–T25): (**a**) impulsive probability PRO_{im}; (**b**) dynamic probability PRO_{dyn}; (**c**) quasi-static probability PRO_{qs+}.

The wave impact on the vertical wall portion was expected to depend on both the incoming wave height and period [8–10,12,13,49]. Figure 12 shows the probability of these three types of wave impact for a clearance equal to c = 0.10 m (trials T31–T35), where the significant wave height H_s was normalized by wave length L (a function of the wave period) on the horizontal axis. For a larger wave steepness (H_s/L), the probability of impulsive processes increased, and the probability of quasi-static processes decreased. The probability of dynamic impact was also variable, increasing with greater wave steepness. In general, at a relatively large wave steepness, PRO_{im} and PRO_{dyn} played the dominant roles.

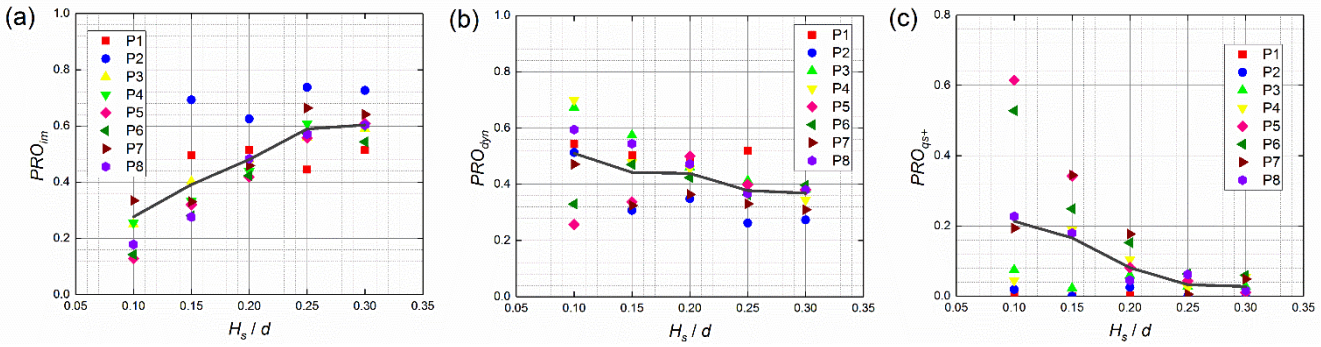

Figure 11. Influence of relative wave height on the probabilities of three types of wave impact on horizontal slab for structural clearance of −0.02 m (trials T11–T15): (**a**) impulsive probability PRO_{im}; (**b**) dynamic probability PRO_{dyn}; (**c**) quasi-static probability PRO_{qs+}.

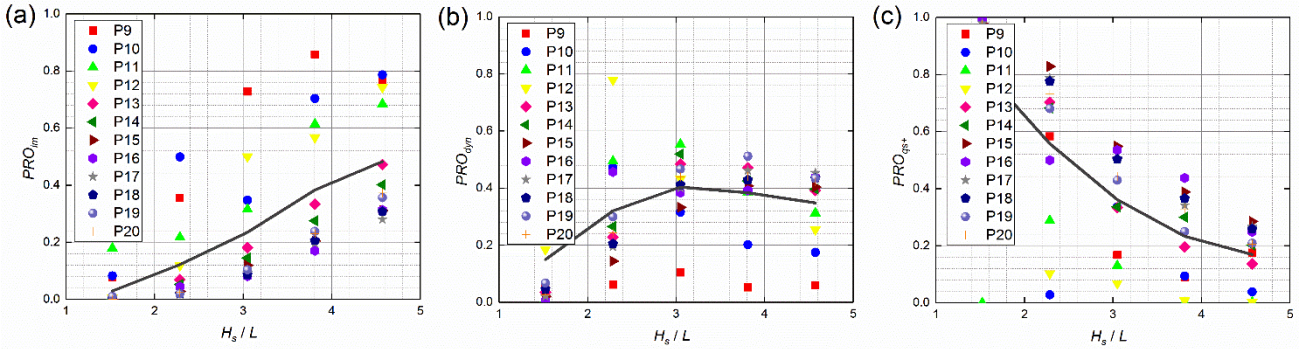

Figure 12. Influence of wave steepness on the probabilities of three types of wave impact on vertical wall for structural clearance of 0.10 m (trials T31–T35): (**a**) impulsive probability PRO_{im}; (**b**) dynamic probability PRO_{dyn}; (**c**) quasi-static probability PRO_{qs+}.

3.3. Effect of Structural Clearance on the Probabilities of Different Wave Impacts

In addition to incident wave conditions, structural clearance also has a significant influence on the wave impact on the vertical wall with an overhanging horizontal cantilever slab [35]. For a constant significant wave height H_s = 0.10 m and period T_p = 1.45 s, Figure 13 illustrates how the probability of different wave impacts varied with different normalized structural clearances (c/H_s), for the horizontal cantilever slab portion of the model (trials T3, T8, T13, T18, T23, T28, and T33). With an increasing structural clearance c/H_s, the impulsive wave impact initially increased and then decreased in proportion, reaching the peak value of around 90% at c/H_s = 0.0–0.2 for the case when there was a relatively thin air layer between the wave surface and the structural bottom. When c/H_s is close to −1.0, the wave surface motion resulted in a negligible occurrence of impulsive impacts, with PRO_{im} dropping to around zero, while the quasi-static and dynamic processes were dominant. As the horizontal slab portion turned from submerged to elevated at c/H_s = 0, the dynamic process rapidly decreased to near zero, and the quasi-static wave impact gradually increased as a result of the decline in impulsive processes. These results indicated that dynamic wave impacts only needed to be taken into account when the slab was below the still water level.

The normalized structural clearance (c/H_s) also had a considerable effect on the probability of the wave impact type on the vertical wall part of the C2 structure. Figure 14 shows how the probabilities of the different wave impact types were influenced by the relative structural clearance, for a constant wave condition H_s = 0.10 m and T_p = 1.45 s (trials T3, T8, T13, T18, T23, T28, and T33). As c/H_s increased, PRO_{im} and PRO_{qs+} of the vertical wall displayed similar general patterns to PRO_{im} and PRO_{qs+} for the horizontal slab. However, compared with results on the horizontal slab, the vertical wall had a large PRO_{qs+} and smaller PRO_{im}, consistent with common damage features of marine structures

in that failures of horizontal parts were usually more severe than those of vertical structures (such as seawalls, coastal bridges, breakwaters, and wharves) [5,24,25]. In addition, the results showed that the role of the dynamic wave impact could not be negligible due to the relatively gentle wave impact on the vertical wall under the water, with PRO_{dyn} ranging between 20% and 60%.

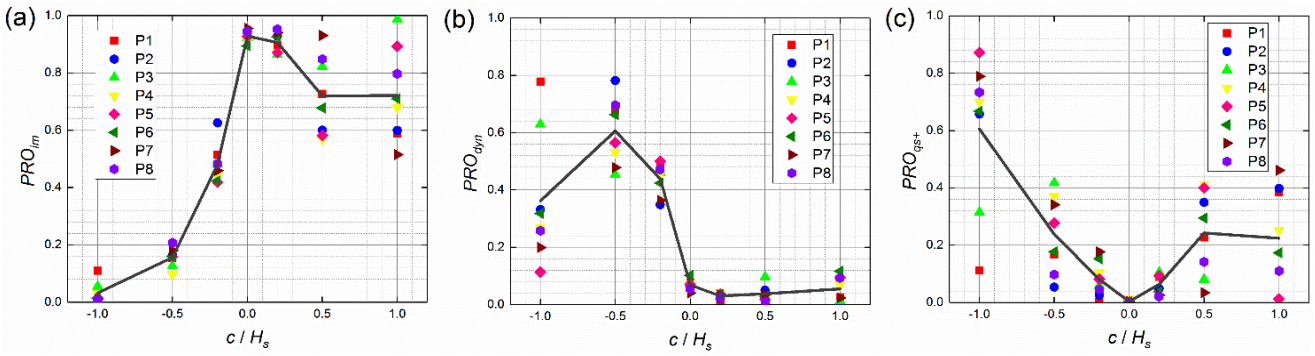

Figure 13. Influence of the relative structural clearance on the probabilities of three types of wave impacts on the horizontal slab portion for incoming significant wave height of 0.10 m (trials T3, T8, T13, T18, T23, T28, and T33): (**a**) impulsive probability PRO_{im}; (**b**) dynamic probability PRO_{dyn}; (**c**) quasi-static probability PRO_{qs+}.

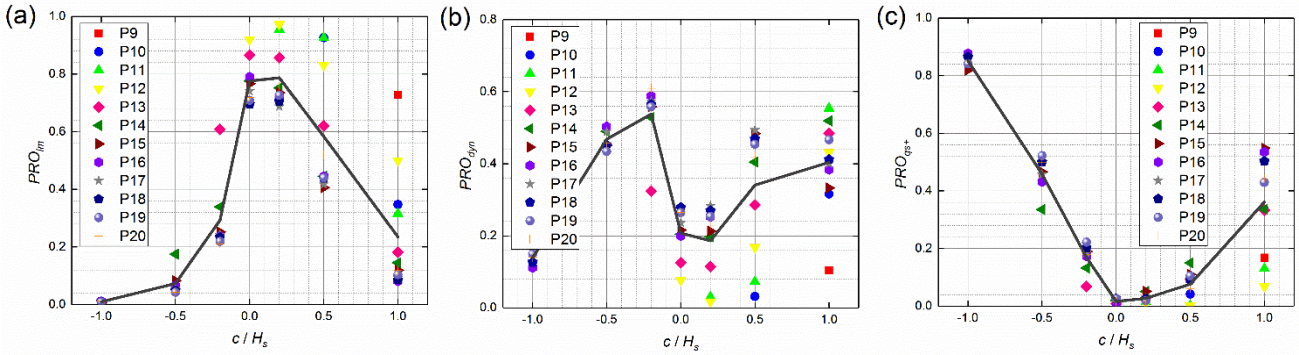

Figure 14. Influence of relative structural clearance (c/H_s) on the probabilities of three types of wave impact on vertical wall portion for incoming significant wave height of 0.10 m (trials T3, T8, T13, T18, T23, T28, and T33): (**a**) impulsive probability PRO_{im}; (**b**) dynamic probability PRO_{dyn}; (**c**) quasi-static probability PRO_{qs+}.

When considering all the results above, it was found that different wave impact types (impulsive, dynamic, or quasi-static) dominated for specific structural clearance ranges. As restricted by the present model test, the relative clearance c/H_s ranged from -1.0 to 1.0 (i.e., within one wave height around the still water level). As summarized in Table 5, when $c/H_s > 0$, both the overhanging slab and vertical wall were dominated by impulsive wave impacts. As the horizontal slab was shifted below the still water level, the entire structure was increasingly affected by the dynamic wave impact. Finally, when $c/H_s < -0.5$, the influence of wave surface motion led predominantly to only quasi-static wave impacts. Although the conclusions above were based on the variation trend of the sensor-averaged probabilities of different wave impact types, and it was shown that a certain part of the slab or vertical wall would be affected by the impulsive wave impacts with the larger probability than the averaged one, the results can still be helpful to preliminarily distinguish the dominant wave impact types under different wave conditions and structural clearances.

Table 5. Classification of dominant wave impact type on relative clearance.

Different Types of Wave Impact	Relative Structural Clearance	
	Horizontal Overhanging Cantilever Slab	Vertical Wall
Impulsive	$c/H_s > -0.20$	$c/H_s > -0.10$
Dynamic	$-0.80 < c/H_s < -0.20$	$-0.50 < c/H_s < -0.10$
Quasi-static	$c/H_s < -0.80$	$c/H_s < -0.50$

Due to the dynamic effects of wave loads during the structural analysis, previous research initially proposed the use of a magnification factor (also called the dynamic magnification factor) to estimate the maximum loads [50]. More recently, studies have proposed categorizing different wave impact loads into three main domains: impulsive, dynamic, and quasi-static [51]. According to the response spectrum of the magnification factor for a linear single degree of freedom model (SDOF) subject to the wave impact, different ranges of magnification factor for three domains were proposed by Chen et al. [31], as summarized in Table 6. In view of this, by referring to the present study results, it can be efficient and time-saving to make a preliminary judgment of the dominant wave impact type, as well as the corresponding magnification effect when designing a structure in the form of a vertical wall with a horizontal cantilever slab (such as flood gates, lock gates, wharves, seawalls, and coastal bridges).

Table 6. Ranges of magnification factor for different wave impact types [31].

Different Types of Wave Impact	Range of Magnification Factor	
	Lower Limit	Upper Limit
Impulsive	0.3	0.7
Dynamic	0.7	1.8
Quasi-static	1	1.8

3.4. Comparison of Wave Impacts between a Horizontal Slab with and without the Vertical Wall

To investigate how the presence of the vertical wall affect wave impacts on the horizontal slab, comparisons of the averaged $P_{1/100}$ and corresponding impulsive wave impact probability between the slab with and without the vertical wall are shown in Figure 15, for wave trials from T16 to T20. Based on the variable wave heights and the fixed water depth in these five trials, the relative significant wave height normalized by the water depth H_s/d is shown on the horizontal axis. The presence of the vertical wall enhanced the wave loads on the horizontal slab by approximately 2–3 times (Figure 15a), which was due to the blocking effect of the vertical wall inducing substantial wave reflection in front of the wall. The addition of the vertical wall also slightly enhanced the impulsive probability PRO_{im} of the slab by about 10%. However, the slab without the vertical wall still presented a large PRO_{im}, up to around 80% for cases in which the clearance was zero. Overall, these results indicated that the presence of the vertical wall had a detrimental effect on the horizontal slab by increasing the magnitude of wave loads and the probability of impulsive wave impacts.

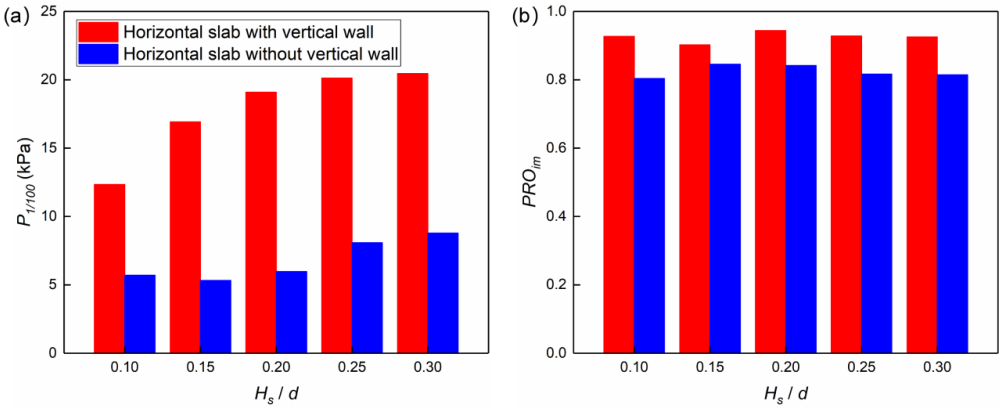

Figure 15. Comparison between the averaged $P_{1/100}$ and the impulsive wave impact probability PRO_{im} for a slab with and without the vertical wall, for trials from T16 to T20: (**a**) the averaged $P_{1/100}$ on the slab; (**b**) impulsive probability PRO_{im}.

4. Conclusions

A vertical wall with an overhanging horizontal cantilever slab has been widely used to assess wave impacts relevant to a wide range of ocean engineering applications, such as predicting maximum forces on surge barriers, flood gates, sluice gates, wharves, and seawalls. During the design process for such marine structures, dynamic effects of wave loads must be considered in the structural analysis, making it imperative to have accurate predictions of the magnitude and frequency of the different wave impact types (impulsive, dynamic, or quasi-static). Wave pressure loads from systematic wave model tests of two configurations (a simple horizontal plate and a vertical wall with a horizontal overhanging cantilever slab) were used to investigate these different wave impact load types. Based on the model test of the simple horizontal plate, a suitable cut-off frequency to separate the quasi-static wave load from the impulsive wave load was established. When applying the low-pass filtering method with a selected cut-off frequency to the pressure time series results for the vertical wall with a horizontal cantilever slab, the study identified the influences of the wave conditions and the structural clearance on the probabilities of these three types of wave impact (impulsive, dynamic, and quasi-static).

The quasi-static uplift wave pressure on the horizontal plate was first evaluated by comparing the predicted values from the empirical formula of Cuomo et al. [24] with the measured pressure time series. When using the reconstructed time series of the quasi-static wave load with different cut-off frequencies, it was found that a cut-off frequency of 7 Hz could reasonably separate the quasi-static component from the impulsive wave impact. This approach was used to classify the individual wave impacts into these three different types (impulsive, dynamic, and quasi-static). For the case of the vertical wall with an overhanging horizontal cantilever slab, both wave conditions and structural clearance were found to have a significant effect on the probabilities of these three types of wave impact. With the increasing wave height and wave steepness, the horizontal slab and vertical wall experienced a larger fraction of impulsive loads and a smaller fraction of quasi-static loads, while the dynamic probability remained stable. When the overhanging slab shifted from elevated to submerged, the dominant wave impact type was more variable. When $c/H_s > 0$, both the overhanging slab and vertical wall were dominated by impulsive wave impacts. When the horizontal slab shifted to a deeper elevation, the entire structure became mainly affected by dynamic wave impacts. Finally, when $c/H_s < -0.5$, the influence of the wave surface motion was weakened so significantly that only the quasi-static wave impact could be observed. Based on these model results, estimates of the occurrences of these different wave impact types can be obtained when designing a range of structures that can be modeled using a vertical wall with a horizontal cantilever slab (such as flood gates, lock gates, wharves, seawalls, and coastal bridges). These results indicated that the presence of the vertical wall had a detrimental effect on the horizontal slab by enhancing the

magnitude of the wave loads and the probability of impulsive wave impacts. In the future, it would be worthwhile to carry out further wave model tests to further expand the related results to different structure geometries and the integrated wave forces, and more detailed measurements of the hydrodynamic processes (e.g., velocity fields) near the structure will be also crucial to strengthen the understanding of the wave–structure interactions.

Author Contributions: Conceptualization, J.H.; methodology, J.H.; validation, J.H.; formal analysis, J.H. and G.C.; investigation, J.H. and G.C.; resources, G.C.; writing—original draft preparation, J.H.; writing—review and editing, R.J.L.; supervision, G.C. and R.J.L. All authors have read and agreed to the published version of the manuscript.

Funding: This research received no external funding.

Institutional Review Board Statement: Not applicable.

Informed Consent Statement: Not applicable.

Data Availability Statement: Not applicable.

Acknowledgments: The authors would like to thank the China Scholarship Council (CSC) for the financial support of this research.

Conflicts of Interest: The authors declare no conflict of interest.

References

1. Meinshausen, M.; Meinshausen, N.; Hare, W.; Raper, S.; Frieler, K.; Knutti, R.; Frame, D.; Allen, M. Greenhouse-gas emission targets for limiting global warming to 2 °C. *Nature* **2009**, *458*, 1158–1162. [CrossRef] [PubMed]
2. Jongman, B.; Ward, P. Global exposure to river and coastal flooding: Long term trends and changes. *Glob. Environ. Change* **2012**, *22*, 823–835. [CrossRef]
3. Mazinani, I.; Ismail, Z.; Hashim, A. An overview of tsunami wave force on coastal bridge and open challenges. *J. Earthq. Tsunami* **2015**, *9*, 1550006. [CrossRef]
4. Zang, Z.; Fang, Z.; Zhang, N. Flow mechanism of impulsive wave forces and improvement on hydrodynamic performance of a comb-type breakwater. *Coast. Eng.* **2018**, *133*, 142–158. [CrossRef]
5. Hayatdavoodi, M.; Ertekin, R. Review of wave loads on coastal bridge decks. *Appl. Mech. Rev.* **2016**, *68*, 030802. [CrossRef]
6. Neumann, B.; Vafeidis, A.; Zimmermann, J.; Nicholls, R. Future coastal population growth and exposure to sea-level rise and coastal flooding—A global assessment. *PLoS ONE* **2015**, *10*, e0118571. [CrossRef]
7. Nicholls, R.; Brown, S.; Goodwin, P.; Wahl, T.; Lowe, J.; Solan, M.; Godbold, J.; Haigh, I.; Lincke, D.; Hinkel, J.; et al. Stabilization of global temperature at 1.5 °C and 2.0 °C: Implications for coastal areas. *Philos. Trans. R. Soc. A Math. Phys. Eng. Sci.* **2018**, *376*, 20160448. [CrossRef]
8. Bagnold, R. Interim report on wave-pressure research. (includes plates and photographs). *J. Inst. Civ. Eng.* **1939**, *12*, 202–226. [CrossRef]
9. Mitsuyasu, H. Shock pressure of breaking wave. *Coast. Eng. Jpn.* **1966**, *9*, 83–96. [CrossRef]
10. Hull, P.; Müller, G. An investigation of breaker heights, shapes and pressures. *Ocean Eng.* **2002**, *29*, 59–79. [CrossRef]
11. Obhrai, C.; Bullock, G.; Wolters, G.; Muller, G.; Peregrine, H.; Bredmose, H.; Grune, J. Violent wave impacts on vertical and inclined walls: Large scale model tests. In Proceedings of the Coastal Engineering, Lisbon, Portugal, 19–24 September 2004.
12. Hofland, B.; Kaminski, M.; Wolters, G. Large scale wave impacts on a vertical wall. In Proceedings of the Coastal Engineering, Shanghai, China, 30 June–5 July 2010.
13. Hu, Z.; Mai, T.; Greaves, D.; Raby, A. Investigations of offshore breaking wave impacts on a large offshore structure. *J. Fluids Struct.* **2017**, *75*, 99–116. [CrossRef]
14. Kirkgöz, M.S. Shock pressures of breaking wave on vertical walls. *J. Waterw. Port Coast. Ocean. Div.* **1982**, *108*, 81–95. [CrossRef]
15. Allsop, N.W.H.; Vann, A.M.; Howarth, M.; Jones, R.; Davis, J.P. Measurements of wave impacts at full scale: Results of fieldwork on concrete armour units. In Proceedings of the ICE Breakwaters Conference, London, UK, 27–29 April 1995; pp. 287–302.
16. Cuomo, G.; Allsop, W.; Bruce, T.; Pearson, J. Breaking wave loads at vertical seawalls and breakwaters. *Coast. Eng.* **2010**, *57*, 424–439. [CrossRef]
17. Marzeddu, A.; Oliveira, T.C.A.; Gironella, F.X.; Sanchez-Arcilla, A. Variability of wave impact measurements on vertical breakwaters. *J. Hydraul. Res.* **2017**, *55*, 772–786. [CrossRef]
18. Goda, Y. New wave pressure formulae for composite breakwaters. In Proceedings of the 14th International Conference on Coastal Engineering, Copenhagen, Denmark, 24–28 June 1974.
19. Cuomo, G.; Tirindelli, M.; Allsop, W. Wave-in-deck loads on exposed jetties. *Coast. Eng.* **2007**, *54*, 657–679. [CrossRef]
20. Istrati, D.; Buckle, I.; Lomonaco, P.; Yim, S. Deciphering the Tsunami Wave Impact and Associated Connection Forces in Open-Girder Coastal Bridges. *J. Mar. Sci. Eng.* **2018**, *6*, 148. [CrossRef]

21. Chen, C.; Melville, B.; Nandasena, N.; Shamseldin, A.; Wotherspoon, L. Experimental study of uplift loads due to tsunami bore impact on a wharf model. *Coast. Eng.* **2016**, *117*, 126–137. [CrossRef]
22. Park, H.; Tomiczek, T.; Cox, D.; van de Lindt, J.; Lomonaco, P. Experimental modeling of horizontal and vertical wave forces on an elevated coastal structure. *Coast. Eng.* **2017**, *128*, 58–74. [CrossRef]
23. Huang, J.; Chen, G. Experimental modeling of wave load on a pile-supported wharf with pile breakwater. *Ocean Eng.* **2020**, *201*, 107149. [CrossRef]
24. Cuomo, G.; Shimosako, K.; Takahashi, S. Wave-in-deck loads on coastal bridges and the role of air. *Coast. Eng.* **2009**, *56*, 793–809. [CrossRef]
25. Castellino, M.; Sammarco, P.; Romano, A.; Martinelli, L.; Ruol, P.; Franco, L.; De Girolamo, P. Large impulsive forces on recurved parapets under non-breaking waves. A numerical study. *Coast. Eng.* **2018**, *136*, 1–15. [CrossRef]
26. Kisacik, D.; Troch, P.; Van Bogaert, P. Description of loading conditions due to violent wave impacts on a vertical structure with an overhanging horizontal cantilever slab. *Coast. Eng.* **2012**, *60*, 201–226. [CrossRef]
27. Kisacik, D.; Troch, P.; Van Bogaert, P. Experimental study of violent wave impact on a vertical structure with an overhanging horizontal cantilever slab. *Ocean. Eng.* **2012**, *49*, 1–15. [CrossRef]
28. Kisacik, D.; Troch, P.; Van Bogaert, P.; Caspeele, R. Investigation of uplift impact forces on a vertical wall with an overhanging horizontal cantilever slab. *Coast. Eng.* **2014**, *90*, 12–22. [CrossRef]
29. Kisacik, D.; Tarakcioglu, G.; Troch, P. Wave-induced uprush jet velocity on a vertical structure. *Ocean Eng.* **2016**, *127*, 103–113. [CrossRef]
30. Martinelli, L.; Ruol, P.; Volpato, M.; Favaretto, C.; Castellino, M.; De Girolamo, P.; Francoc, L.; Romanob, A.; Sammarco, P. Experimental investigation on non-breaking wave forces and overtopping at the recurved parapets of vertical breakwaters. *Coast. Eng.* **2018**, *141*, 52–67. [CrossRef]
31. Chen, X.; Hofland, B.; Molenaar, W.; Capel, A.; Van Gent, M. Use of impulses to determine the reaction force of a hydraulic structure with an overhang due to wave impact. *Coast. Eng.* **2019**, *147*, 75–88. [CrossRef]
32. De Almeida, E.; Hofland, B. Validation of pressure-impulse theory for standing wave impact loading on vertical hydraulic structures with short overhangs. *Coast. Eng.* **2020**, *159*, 103702. [CrossRef]
33. De Almeida, E.; Hofland, B. Experimental Observations on Impact Velocity and Entrapped Air for Standing Wave Impacts on Vertical Hydraulic Structures with Overhangs. *J. Mar. Sci. Eng.* **2020**, *8*, 857. [CrossRef]
34. De Almeida, E.; Hofland, B. Standing wave impacts on vertical hydraulic structures with overhangs for varying wave fields and configurations. *J. Coast. Hydraul. Struct.* **2021**, *1*, 1–24.
35. Huang, J.; Chen, G. Experimental study on wave impulse and characteristic pressure of a vertical wall with overhanging horizontal cantilever slab. *Ocean Eng.* **2020**, *217*, 108055. [CrossRef]
36. Huang, J.; Chen, G. Experimental study of wave impact on a vertical wall with overhanging horizontal cantilever slab and structural response analysis. *Ocean Eng.* **2022**, *247*, 110765. [CrossRef]
37. Anagnostopoulos, S. Dynamic response of offshore platforms to extreme waves including fluid-structure interaction. *Eng. Struct.* **1982**, *4*, 179–185. [CrossRef]
38. Istrati, D.; Buckle, I. Effect of fluid-structure interaction on connection forces in bridges due to tsunami loads. In Proceedings of the 30th US-Japan Bridge Engineering Workshop, Washington, DC, USA, 21–23 October 2014.
39. Choi, S.; Lee, K.; Gudmestad, O. The effect of dynamic amplification due to a structure's vibration on breaking wave impact. *Ocean Eng.* **2015**, *96*, 8–20. [CrossRef]
40. Brito, M.; Ferreira, R.; Teixeira, L.; Neves, M.; Canelas, R. Experimental investigation on the power capture of an oscillating wave surge converter in unidirectional waves. *Renew. Energy* **2020**, *151*, 975–992. [CrossRef]
41. Brito, M.; Ferreira, R.; Teixeira, L.; Neves, M.; Gil, L. Experimental Investigation of the Flow Field in the Vicinity of an Oscillating Wave Surge Converter. *J. Mar. Sci. Eng.* **2020**, *8*, 976. [CrossRef]
42. Kortenhaus, A.; Oumeraci, H. Classification of wave loading on monolithic coastal structures. In Proceedings of the 26th International Conference on Coastal Engineering, Copenhagen, Denmark, 22–26 June 1998.
43. Streicher, M.; Kortenhaus, A.; Marinov, K.; Hirt, M.; Hughes, S.; Hofland, B.; Scheres, B.; Schüttrumpf, H. Classification of bore patterns induced by storm waves overtopping a dike crest and their impact types on dike mounted vertical walls—A large-scale model study. *Coast. Eng. J.* **2019**, *61*, 321–339. [CrossRef]
44. Jose, J.; Podrazka, O.; Obhrai, C.; Gudmestad, O.; Cieslikiewicz, W. Methods for analysing wave slamming loads on truss structures used in offshore wind applications based on experimental data. *Int. J. Offshore Polar Eng.* **2016**, *26*, 100–108. [CrossRef]
45. Istrati, D.; Buckle, I. Role of trapped air on the tsunami-induced transient loads and response of coastal bridges. *Geosciences* **2019**, *9*, 191. [CrossRef]
46. Seiffert, B.; Ertekin, R.; Robertson, I. Wave loads on a coastal bridge deck and the role of entrapped air. *Appl. Ocean Res.* **2015**, *53*, 91–106. [CrossRef]
47. Thomson, R.; Emery, W. *Data Analysis Methods in Physical Oceanography*, 3rd ed.; Elsevier: Amsterdam, The Netherlands, 2014.
48. Xiang, T.; Istrati, D.; Yim, S.; Buckle, I.; Lomonaco, P. Tsunami Loads on a Representative Coastal Bridge Deck: Experimental Study and Validation of Design Equations. *J. Waterw. Port Coast. Ocean. Eng.* **2020**, *146*, 04020022. [CrossRef]
49. Oumeraci, H.; Klammer, P.; Partenscky, H. Classification of breaking wave loads on vertical structures. *J. Waterw. Port Coast. Ocean. Eng.* **1993**, *119*, 381–397. [CrossRef]

50. Oumeraci, H.; Kortenhaus, A. Analysis of the dynamic response of caisson breakwaters. *Coast. Eng.* **1994**, *22*, 159–183. [CrossRef]
51. Humar, J. *Dynamics of Structures*, 3rd ed.; CRC Press: Boca Raton, FL, USA, 2012.